Hypersonic jets in astrophysical conditions: focus on spreading and asymmetric stability properties

2014 New J. Phys. 16 085002

(http://iopscience.iop.org/1367-2630/16/8/085002)

New Journal of Physics
The open access journal at the forefront of physics
Deutsche Physikalische Gesellschaft DPG | IOP Institute of Physics

Hypersonic jets in astrophysical conditions: focus on spreading and asymmetric stability properties

M Belan[1], D Tordella[2], S De Ponte[3], A Mignone[4] and S Massaglia[4]

[1] Politecnico di Milano, Dipartimento di Scienze e Tecnologie Aerospaziali, Italy
[2] Dipartimento di Ingegneria Meccanica e Aerospaziale, Politecnico di Torino, Italy
[3] retired, formerly Politecnico di Milano, Dipartimento di Scienze e Tecnologie Aerospaziali, Italy
[4] Dipartimento di Fisica, Università di Torino, Italy
E-mail: marco.belan@polimi.it

Received 18 March 2014, revised 13 May 2014
Accepted for publication 2 June 2014
Published 7 August 2014

New Journal of Physics **16** (2014) 085002

doi:10.1088/1367-2630/16/8/085002

Abstract

High Mach number jets emanating from young stars show remarkable collimation, low opening angle and resilience against the growth of instabilities, especially the asymmetric ones. In recent laboratory experiments instances of asymmetric three-dimensional low amplitude long waves aligned with the jet axis were observed by Belan *et al* (2013 *Astron. Astrophys.* **554** A99). To explore the collimation, spreading, and asymmetric stability properties of hypersonic jets we carried out laboratory experiments and numerical simulations in two and three spatial dimensions. We find that laboratory hydrodynamic jets with high Mach numbers remain collimated, for hundreds of jet radii in length and maintain low opening angles. These findings are confirmed by 3D numerical simulations carried out after time-dependent, asymmetric perturbations are applied at the jet inlet. Both experimental and perturbed simulated jets show non-axial modes with long wavelengths, whose growth does not disrupt the jet in the domain considered.

Keywords: hypersonic jets, stellar jets, jet stability

1. Introduction

Among the astrophysical phenomena that involve high velocity matter flows, jets are the most widespread in the universe. They are found in the most diverse environments and show a wide range of sizes and powers. At one end, we have jets from active galactic nuclei (AGNs) that are the largest in size, up to a few megaparsecs in length, and the most powerful ones (kinetic power up to $\sim 10^{47-48}$ ergs s^{-1}, (Godfrey and Shabala 2013, see also HD simulations by Zanni *et al* 2003 and Hodges-Kluck and Reynolds 2011). At the other end, we have jets from young stellar objects (YSOs) that are located inside the giant molecular clouds present in our galaxy, and in other ones as well. YSO jets are up to some parsecs long and attain kinetic powers up to $\sim 10^{33}$ ergs s^{-1} (Reipurth and Bally 2001 for a review and recent observations by Hartigan *et al* 2011). While AGN jets have relativistic velocities, YSO jets speeds are the typical escape velocity from stars of a few solar masses, and amount to a few hundreds kilometers per second, corresponding to Mach numbers in the range 10–40. A striking characteristic of jets is their high degree of collimation, in particular YSO jets have opening angles that vary between 0.5° to 5° (Mundt *et al* 1991, Ray *et al* 1996).

In recent years, we have seen many laboratory experiments that try to reproduce some aspects of the jet phenomenology, with particular concern towards YSO jets. These aspects are mainly related to the jet origin, propagation and emission (Bellan *et al* 2005, 2009, Falize *et al* 2011, Gregory *et al* 2008, González *et al* 2009, Hartigan *et al* 2009, Lebedev *et al* 2005, Suzuki-Vidal 2010, Rus *et al* 2002).

With the goal to address the propagation of YSO jets and their interaction with the ambient medium, Tordella *et al* (2011) (paper I) and Belan *et al* (2013) (paper II) studied in the laboratory and by numerical means hypersonic hydrodynamic (HD) flows. In paper I the authors considered as main jet parameters the Mach number M and the jet-to-ambient density ratio η and studied, both experimentally and numerically, representative cases of high and small values of density ratio. In paper II they analyzed several cases with Mach number and density ratios consistent with those derived from the observations of YSO jets.

In this paper we focus our attention on the measure of the spreading of the laboratory jets and the comparison with the results obtained by numerical simulations. We also discuss the appearance of sinuous structures observed in some laboratory jets and the extent to which these features may develop as the response to non-axial perturbations in numerical simulations.

The plan of the paper is the following: in section 2 we outline laboratory and numerical setups, in section 3 we carry out the data analysis and in section 4 we discuss the results. Conclusions are drawn in section 5.

2. Experimental and numerical setups

2.1. The experimental setup

The laboratory experiment makes use of facilities designed and built specifically for studying free hypersonic jets. The main features of these facilities, described in detail in the works by Belan *et al* (2008, 2010, 2011, 2013), will be exposed in this section. The jets studied in the present work are generated by means of de Laval nozzles; they travel along the longitudinal axis of a cylindrical vacuum vessel, as shown in figure 1.

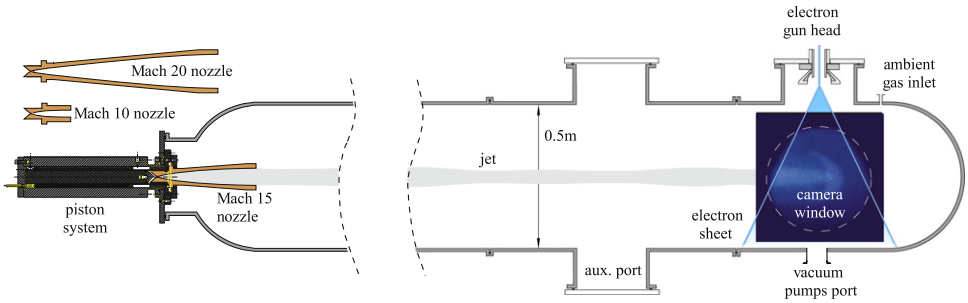

Figure 1. Experiment setup. The modular vessel length depends on the number of assembled sections. The available set of de Laval nozzles is shown on the left (Belan *et al* 2013).

The aim of the present experiment is the scaled simulation of the jet region starting from thousands of AU from its early origin and extending over very long distances. Thus, a suitable device is mandatory to reproduce the right fluid dynamic properties of the flow entering the region of study; this device is in the present setup the de Laval nozzle, and should not be intended as a model for the very near jet zone, where the acceleration of the flow takes place as a consequence of complicated phenomena in the star-disk region, already considered by some of the authors of this work in their previous research (Matsakos *et al* 2008, Tzeferacos *et al* 2009, Zanni *et al* 2007). In particular, the de Laval nozzles permit to reproduce some important properties, including a very small initial spreading angle.

The nozzles in this setup are designed for monoatomic gases flows, considering boundary layer and heat exchange effects, so as to account for the real flow properties. In this study, three de Laval nozzles are available, each one being designed for a nominal Mach number (M = 10, 15, 20). The corresponding flows can be obtained by imposing a given stagnation-to-ambient pressure ratio p_0/p_a. When a nozzle works at this pressure ratio, the output jet has a pressure p_j *matched* to the ambient pressure p_a. It should be recalled, that de Laval nozzles are capable to create quasi–isentropic jets, that is jets devoid of shocks near the nozzle exit sections. In general, it is also possible to adjust the pressure ratios in a limited range without spoiling the main morphology of a jet. This is achieved by varying the jet pressure approximately on the interval $0.8p_a < p_j < 1.2p_a$. Under these conditions, the jets are identified as *nearly matched*.

The use of nearly pressure-matched nozzles relies on the assumption that the near jets are generated as shock–free as they come from the mentioned region close to the star. The hypothesis of pressure equilibrium has been also adopted by other authors (e.g., Borkowski *et al* 1997, de Colle and Raga 2006), arguing that a jet naturally attempts to come in pressure balance with the environment by varying its diameter accordingly. However, this hypothesis is not so restrictive, since the authors of this work has already proven that even jets having unmatched p_j/p_a ratios may exhibit remarkable collimations over long distances. In particular, a case of a slightly unmatched jet is reported in paper II and many cases of highly underexpanded jets having $p_j/p_a \gg 1$ are reported by Belan *et al* (2010).

In the present setup, the jet gas enters the nozzle after being compressed by a fast piston system, which brings the gas to the required stagnation pressure p_0. This pressure may range from 0.04 to 0.7 MPa. The piston raises also the gas temperature, leading to an increase of the

gas enthalpy. Thanks to the high precision machining of the piston, the curves of mass flow versus time are well characterized (paper I), so that the jets under test can be reproduced with a very good repeatability.

The vacuum vessel is modular, different cylindrical sections of diameter 0.5 m are available: they can be assembled together, giving a maximum useful internal length of 3.28 m. For the higher Mach number cases, to study the jets morphology over long distances, a longer size is needed, because of the larger jet diameter. This requirement is satisfied by assembling the required sections to the vessel (see paper II). In all tests, the vacuum vessel diameter is always larger than the jets diameter, thus wall effects can be neglected and the jets travel as free jets until they hit the vessel's end (see paper I). The pressure inside the vessel is maintained by pumps that can reach an ambient level of the order of 1 Pa, this pressure is acquired by means of 0.25% accuracy transducers. The chamber ambient is filled by a gas which can be different from the jet gas and the relevant pressure is controlled by solenoid valves, so that the desired ambient pressure and density can be easily set. The operating range for the ambient pressures ranges from 1.5 to 100 Pa. Since the jet and the ambient can be made of different gases, the jet-to-ambient density ratio $\eta = \rho_j/\rho_a$ can be set independently from the Mach number over a wide range. In particular, it is possible to create jets from underdense conditions ($\eta < 1$) to very overdense conditions ($\eta \gg 1$).

The visualizations, as well as the measurements are mainly obtained by means of the electron beam method based on an electron gun purposely designed and built in the laboratory. The available electron beam, adjustable up to 2 mA at 20 kV, takes the shape of an electron sheet thanks to a deflection system; the electron sheet can be driven to intercept the jet, generating a plane fluorescent section of the flow under consideration. These fluorescent planes are acquired as digital images by a fast intensified camera, working at speeds up to 8000 frames per second. The image resolution is typically 512 × 512. The first results of this technique are visualizations, but image processing techniques are also used to obtain measurements of gas densities and structure velocities (papers I and II). In particular, the gas densities are obtained as functions of the local image intensity, whereas the velocities are obtained by suitable correlation techniques, applied to the typical traveling structures appearing in the jet morphology (for instance, the head bow shock).

Finally, it should be noted that this experimental setup cannot reproduce radiative effects in the jets evolution, whereas the similarity of Mach number and density ratio remains well satisfied. The well known issue of the radiation effects has been already considered by some of the authors of this paper (Tesileanu *et al* 2008) by a numerical approach. However, the piston system used in this facility gives moderate stagnation enthalpies, so that after the expansion developed in the nozzles, the jets travelling in the vessel are always colder than the surrounding ambient, and this prevents the reproduction of radiative effects in the jets evolution. The problem could be solved only by a complicated and expensive improvement of jet generation device.

2.2. The numerical setup

In paper II we have shown that the ideal HD Euler equations are a good approximation to describe the physical conditions of the experimental jet. We have thus solved the HD equations by numerical means employing the PLUTO code by Mignone *et al* (2007) (http://plutocode.ph.unito.it/). The code provides a multiphysics, multialgorithm modular environment which is

particularly oriented towards the treatment of astrophysical flows in the presence of discontinuities. In this case, among the different modules and algorithms available, Newtonian ideal HDs was used. This module exploits a general framework to integrate a system of conservation laws, built on modern Godunov-type shock-capturing schemes.

In this study we numerically analyze the jet spreading properties by using the same data set presented in paper II for the 2D cylindrical geometry. Instead, for the nonlinear study of perturbation evolutions for $M = 20$, we have performed 3D simulations anew. These simulations were performed on a 3D domain in Cartesian coordinates $(x,\ y,\ z)$ in units of the initial *effective* jet radius r_0 defined in section 3. The y axis represents the longitudinal direction of the jet. The boundary, initial and injection conditions for the jets are described in paper I (see in particular section 2.2 and appendix D). The computational domain is defined by $-12.5 \leqslant (x, z) \leqslant 12.5$ (in the transverse direction) and $0 \leqslant y \leqslant 150$ (in the longitudinal direction). We employ a uniform grid resolution of $256 \times 256 \times 1512$ zones, respectively.

In addition, for studying the sinuous behaviour shown in the laboratory for the case $M = 20$ (see figure 7), we have superimposed at the jet injection a time-dependent perturbation to the transverse jet velocity components of the form:

$$(v_x,\ v_z) = \epsilon \cos(m\phi + \omega t)(\cos\phi,\ \sin\phi)\ , \tag{1}$$

with $\phi = \tan^{-1}(z/x)$ and the azimuthal wave number $m = 1$. The perturbation amplitude ϵ and the frequency ω have been inferred empirically by inspecting the sinuous structure visible in a laboratory jet (figure 7), in particular $\omega = 2\pi/T$ corresponds to a period $T = \lambda/v_j$ where λ and v_j are the wavelength and the jet velocity. Explicit values of ϵ and λ may be found in section 4.2.

3. Data analysis

A large set of jets has been studied in this experiment: the Mach numbers range from 7 to 21, and the density ratios η from 0.5 to more than 100. Some of these have also been compared with the corresponding numerical simulations.

Figure 2 represents the set of configurations considered in the present experimental campaign, labelled by the two main parameters M and η. The nozzles and the pair of gases (jet-ambient) used for each test are also reported. The dashed line on the left side marks the boundary of a region where the low Reynolds number effects are so important that the experiments cannot give reliable results, since the physics is in that case dominated by the molecular diffusion, in such a way that the jets can also be destroyed on a short scale by the mixing with the ambient and the associated kinetic energy dissipation. The dotted line on the right side marks the boundary of a region where both Mach number and density ratio are so large that the behaviour of the jets tends to resemble the motion of a rigid column.

For the sake of quantifying the jet spreading and its dependence on the control parameters, suitable comparison criteria should be identified. A first step is the definition of a jet radius, holding along the whole jet length. This definition should be consistent with the jet generation process. Actually, the jets are originated by solid wall nozzles and the presence of a diffusive boundary layer of non-negligible thickness must be considered. By observing that in the present experiment the information is mainly obtained from measurements of light emission intensity, a proper definition for the jet radius r_j can be given in terms of density variations across the jets, since the emitted light is directly related to the gas density.

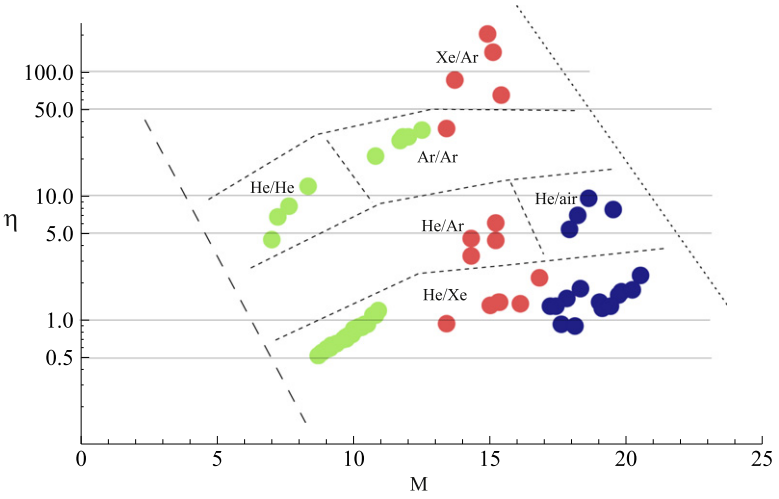

Figure 2. Mach–η parameter space. Each circle represents a single experiment, the relevant setup is indicated by the circle colors. Green circles: Mach 10 nozzle. Red circles: Mach 15 nozzle. Blue circles: Mach 20 nozzle. Below the dashed line, the experiments are heavily influenced by the low Reynolds number. Above the dotted line, Mach number and density ratio are very high, beyond the scope of the present research. Short–dashed lines separate regions of the parameter space where different pairs of jet/ambient gases have been used.

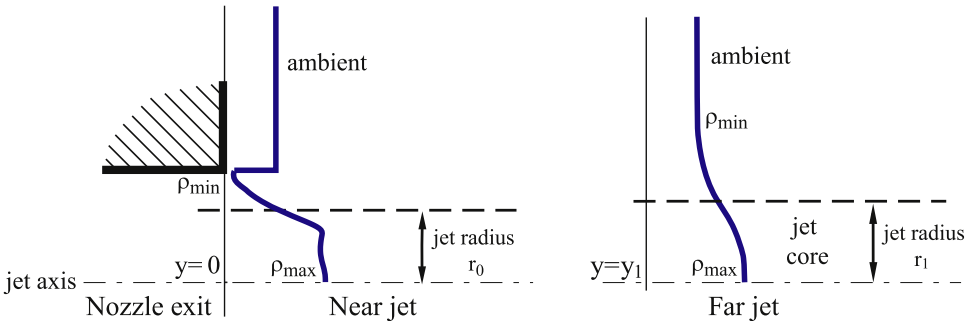

Figure 3. Jet width measurement technique for overdense jets. The far field profile is sketched for $y_1 \gg r_0$.The conventional jet radius is taken at the points where the density is reduced by 0.5 times the difference between the axial value and the lateral minimum. The density minimum is found near the wall at the nozzle exit when considering the near field region and in the outer ambient region when considering the far field.

The jet radius is thus defined as the distance from the axis at which the density is reduced by 0.5 times the difference between the axial value and the local minimum value observed in the outer zone along the jet radial direction, see figures 3 and 4:

$$r_j = r\left[\rho = \rho_{\min} + \frac{1}{2}(\rho_{\max} - \rho_{\min})\right]. \tag{2}$$

This definition is a generalized form of the *half density–half width* criterion and can be easily extended to the far field assuming as jet radius the point of half width between the central (axial) maximum and the local external minimum found marching along the radial direction.

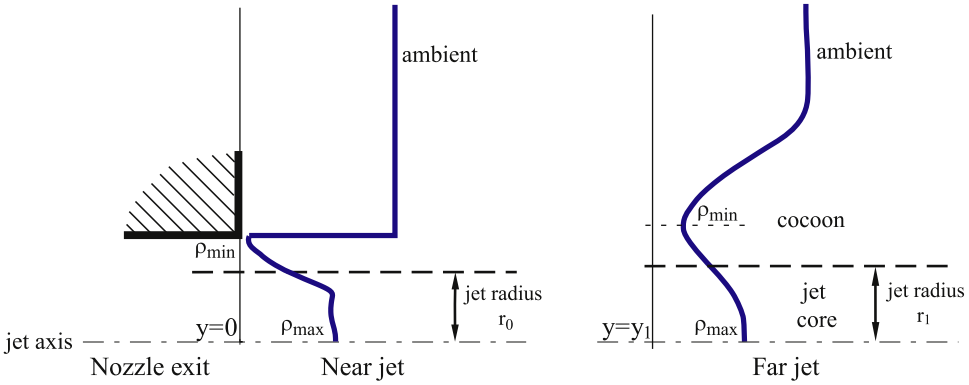

Figure 4. Jet width measurement technique for underdense jets. The conventional jet radius is taken at the points where the density is reduced by 0.5 times the difference between the axial value and the lateral minimum. The density minimum is found near the wall at the nozzle exit when considering the near field region and in the cocoon region when considering the far field.

The concept is illustrated in figure 3: at the nozzle exit ($y = 0$), the jet radius assumes a value r_0 which is smaller than the nozzle radius because of the boundary layer. The quantity r_0 is also useful as a reference length (jet initial radius) and as a basis for the definition of the time scale $\tau = r_0/c_0$ where c_0 is the speed of sound at the center of the nozzle exit. The definition of r_0 relies on the numerical knowledge of the flow at the nozzle output, as described by Belan *et al* (2001). At a given downstream distance y_1, the same criterion can be used to quantify a new jet radius r_1. In these experiments, y_1 is always chosen in the far field ($100r_0 < y_1 < 200r_0$), avoiding the jet head zone. This definition for the jet radius holds for any value of the density ratio, as shown in figure 4, that represents the development of an underdense jet from the nozzle to the far field. It is worth noting that the jet radius introduced here has a relative and not absolute meaning (other quantities proportional to r_0 could be taken as conventional jet radii without any loss of generality when similar jets are compared).

As a further step, an estimation of the jet spreading can be obtained by considering the increase of the jet radius along the axis

$$\delta_r(y) = r_1(y) - r_0. \tag{3}$$

Once a longterm distance consistent with the apparatus characteristics and a feasible laboratory measure of the lateral jet spreading is defined, it is possible to calculate the spreading angle through the ratio

$$\alpha = 2 \arctan\left(\delta_r/y_1\right). \tag{4}$$

It is important to remark that these measurements are averaged in time over tens of time scales, i.e., the jet radius or width are measured at a fixed point while the jet structures move. Varicose and sinuous instabilities may appear, but a mean value for the jet width can always be determined, provided that the time–average window is long enough as to give steady results.

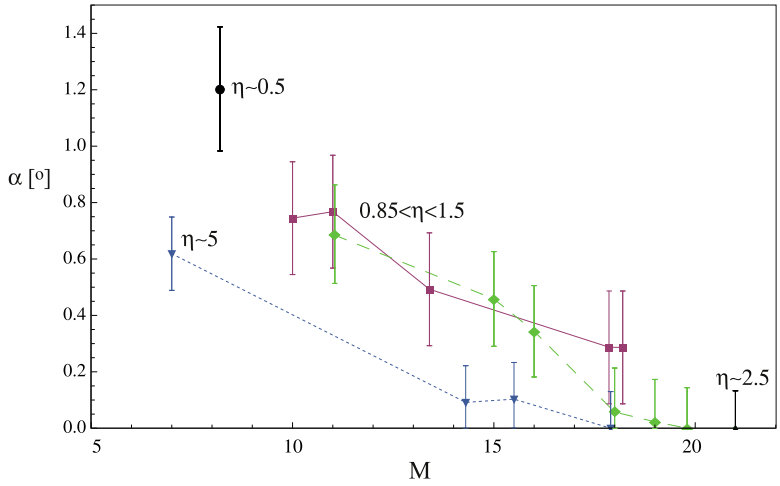

Figure 5. Spreading measurements: spreading (opening) angles as functions of the Mach numbers for different density ratios. The figure includes: (1) a set of data from jets having density ratios $\eta \sim 0.9$ (red line); (2) a set of data from jets having density ratios $\eta \sim 1.4$ (green line); (3) a set of data from jets having density ratios $\eta \sim 5$ (blue line); (4) two isolated points for $\eta = 0.5$, M = 8 and $\eta = 0.5$, M = 21 (black points). At the highest Mach numbers, some spreading angles measurements give values very close to zero, so that the relevant error bars are bounded between 0 and a positive value.

4. Results

4.1. Spreading measurements

For a set of 16 jets having different density ratios, spreading measurements versus the Mach number are presented in figure 5 in terms of the difference between the far field radius and nozzle exit radius. The results presented here are obtained from a subset of the test cases shown in figure 2. The jets in the subset have been chosen because of their reasonable accuracies on the spreading measurements; instead, in the worst cases the error bars can be very large and the relevant measurements can not be validated. The heights of the error bars depend on different effects, namely, the image noise and blur (intrinsic to the measurement method, see in paper I, appendix D.2) and the jet diameter variations due to the unsteady structures traveling through the measurement zone.

The comparison between experiments and simulations is possible on 9 known jet configurations (paper II) corresponding to 3 sets, each one with similar density ratio η but different Mach numbers. Here the same algorithm is applied to laboratory images and numerical density maps, the results are shown in figure 6. As expected, the error bars of the time–averaged numerical values are smaller than the relevant laboratory data, but their height is not negligible, because of the variations in the jet diameter due to fluid instabilities.

4.2. Spreading and core instabilities

The averaged method introduced to measure the spreading can give an *estimate* of the effective opening angle of the jets whereas it does not give local—in space or time—information about the variations of the jet diameter. These variations are due to the structures travelling along the

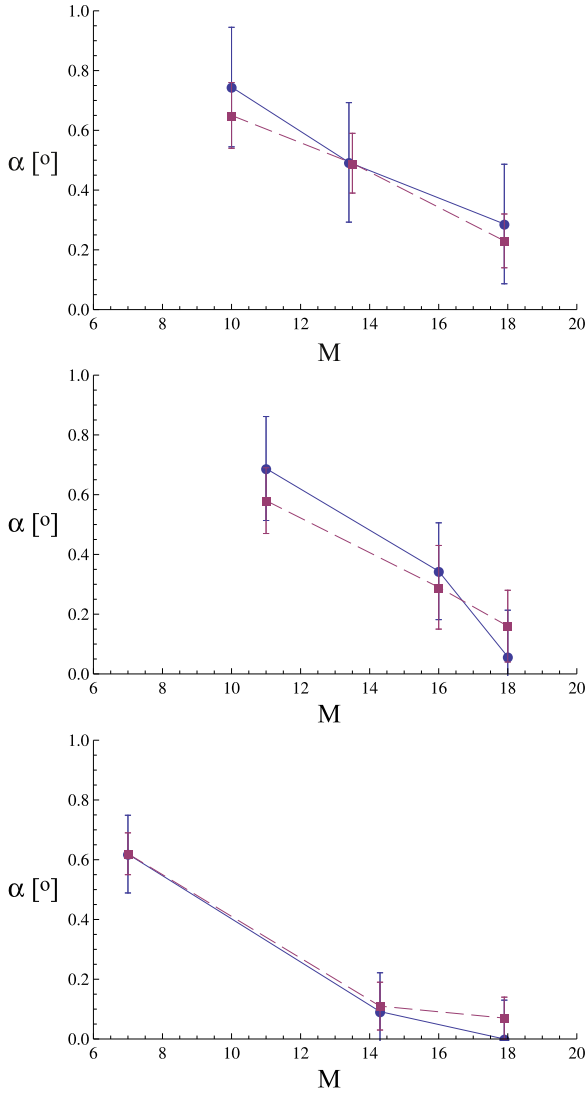

Figure 6. Spreading: comparison between experiments and simulations for 9 known jet configurations (Belan *et al* 2013). From top to bottom: spreading angles versus Mach numbers for different $\eta \sim 0.9$, 1.4 and 5, respectively. Blue: experiments, red: numerical simulations.

jet core, and could be classified as 2D or 3D. In particular, the inherently bi-dimensional axisymmetric structures could be typically compression zones, shocks and expansions due to the jet-to-ambient pressure ratio and to the beam pumping phenomenon (Kössl and Müller 1988, Massaglia *et al* 1996). These structures can be reproduced by our 2D numerical simulations. The inherently three-dimensional structures can have several forms, as sinuous waves, swirled perturbations (corkscrew–like), and so on. For the reproduction of these structures, 3D simulations are necessary. The above classification refers only to large structures, because the small ones, typically related to the turbulent structures, are always 3D.

Figure 7 shows a jet of helium in xenon ambient, having Mach number 19 and $\eta = 1.4$, which exhibits non-axisymmetric large structures. Owing to the experimental technique, the light intensity is proportional to the local gas density; the presented image is obtained as a

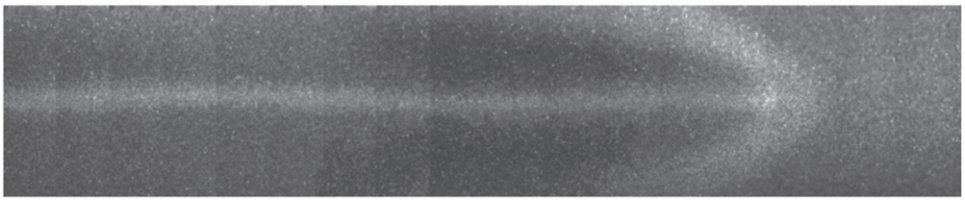

Figure 7. A He in Xe jet ($M = 19$, $\eta = 1.4$) with non-axisymmetric large structures. The image is obtained extracting frames from a movie along a time window of 17 time units τ as explained in the body text.

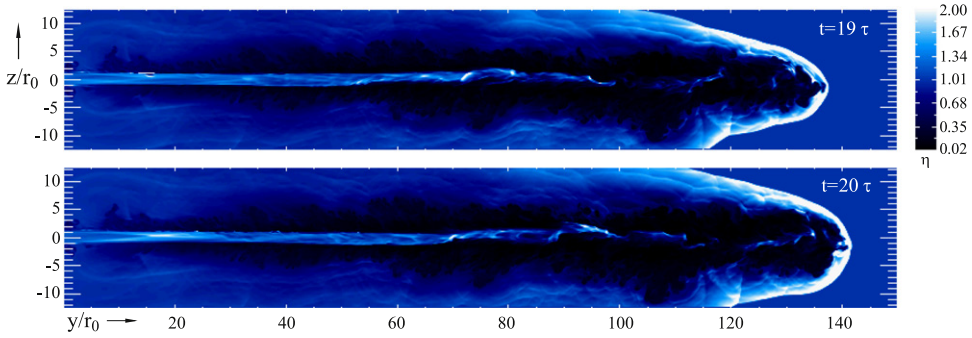

Figure 8. Density distribution image from a 3D simulation of the same case as in figure 7, taken at $t = 19$ and 20 time units, with perturbation amplitude $\epsilon = 0.2$ times the initial on-axis sound speed. Space and time scale, as defined in section 3 are $r_0 = 20.1$ mm and $\tau = 0.16$ ms.

juxtaposition of time-correlated frames on a short time range (papers I and II), in this case 17 time units. The origin of the structures in figure 7 can be related to spontaneous small departures from the axial symmetry of the flow in the injection phase. The visualization of a longitudinal section of the jet is always obtained by a thin electron sheet, so that both the cases of a sinuous and a fully 3D structure are possible, even if the case of a sinuous longitudinal oscillation of the axis entirely contained in a plane is unlikely, since the alignment of this plane with the electron sheet could only accidentally happen.

The treatment of the case exposed above requires a numerical simulation that includes a perturbation superimposed to the boundary conditions at the jet origin, i.e. at the nozzle output location: here the perturbation has been modeled according to equation (1) and the relevant results are shown in figures 8 and 9, which represent simulations for the jet of figure 7 obtained with the same kind of perturbation, but with different amplitudes. We have applied perturbation amplitudes $\epsilon = 0.2$ and 0.05 times the initial on-axis sound speed value for the cases in figure 8 and in figure 9, respectively. The values for v_j and λ, that give ω in equation (1), have been set to 2000 m^{-1} s and 2 m, respectively, in agreement with the experimental values.

4.3. Experiments versus numerical simulations

A large part of the presented results is based on comparisons between experimental and numerical data. The experimental images are essentially light intensity maps, where the light emission is locally proportional to the gas density, and each experimental image is obtained as a

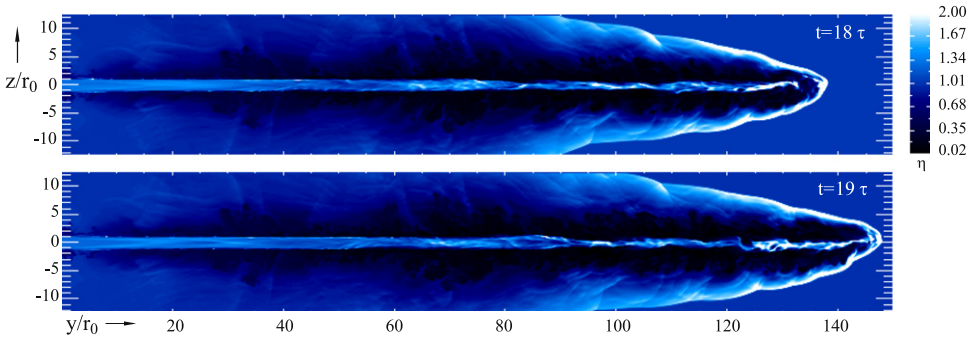

Figure 9. The same as in figure 8 but with $\epsilon = 0.05$ times the initial on-axis sound speed.

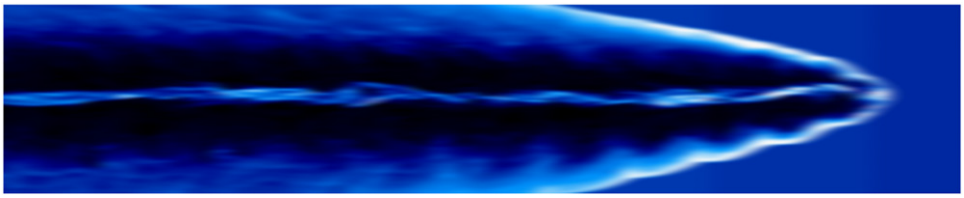

Figure 10. Numerical reconstruction for the jet in figure 7, not to scale, obtained by the same reconstruction method used for the experimental frames, applied to the numerical frames calculated for the small perturbation case as in figure 9. See D2 in paper I.

juxtaposition of time-correlated frames on a short time range including the instant chosen for the corresponding numerical image. The juxtaposition is performed over a limited number of frames, in order to avoid a frozen representation of the jet under test (papers I and II). The numerical images instead are fixed-time representations of the same jets over the complete spatial domain, plotted as density maps.

The validity of the reconstruction method used for experimental results, based on frames juxtaposition, can be checked by introducing a test on the available numerical images as shown in figure 10. Here a juxtaposition of numerical frames on a domain $(107 \times 21)\, r_0$ is presented, obtained over a time interval $15 < t/\tau < 24$ and horizontally blurred by a Gaussian filter over a scale similar to the experimental one, in the order of r_0. In other words, in this test a sequence of numerical frames is treated by the same reconstruction method used for the experimental frames, and the result shows that the jet reconstruction remains realistic.

5. Conclusions

We have examined two basic aspects of the propagation of hypersonic jets: spreading and stability. Observations (see e.g., the review by Reipurth and Bally 2001) point out that jets from YSOs have an observational Mach number ranging from 10 to 40, a jet-to-ambient density ratio in between 1 and 10 and a Reynolds number exceeding 10^{10}. Although in this laboratory experiment the length scales are very different from astrophysical systems, two critical dimensionless parameters, such as the Mach number and the density ratio, have similar values. And the parameters that are larger in astrophysical systems, such as the Reynolds number, are

sufficiently large for the experiment to capture the asymptotic behaviour. Moreover, it should be noted that, as long as radiation transport and relativistic and magneto-hydrodynamic effects can be ignored in the astrophysical situation of interest, the scaling between the experimental system and the corresponding astrophysical systems will primarily depend on the internal Mach number of the jet and on the density ratio, that can be reproduced by the present setup. On the other hand, in this experiment the radiative effects cannot be considered because of the limitations of the present setup, which is a low energy density facility.

Our results indicate that the spreading decreases with the jet Mach number and becomes smaller for heavier jets. The resulting jet opening angle remains well within the variability range observed in jets from YSOs.

Starting from non-axially symmetric oscillations, observed in paper II for high Mach number jets, we have carried out 3D numerical simulations for testing the onset and the nonlinear evolution of potentially disruptive asymmetric modes. We have imposed two different values of the initial perturbation amplitude and transverse velocity and found that the jet was undergoing non-axial oscillations but maintained its integrity for the length of the domain.

Finally, in order to test the consequences of the main limitation of the diagnostics technique, that is the possibility of observing a limited fraction of the jet, we have performed a test case by treating the simulated data with the same juxtaposition technique used for the laboratory data. By comparison with the original figure, we have verified that this technique leads to a reasonable representation of the actual jet propagation details.

References

Belan M, De Ponte S and Tordella D 2008 *Exp. Fluids* **45** 501–11

Belan M, De Ponte S and Tordella D 2010 *Phys. Rev.* E **82** 026303 2

Belan M, De Ponte S, Tordella D, Massaglia S, Ferrari A, Mignone A and Bodenschatz E 2011 *Astrophys. Space Sci.* **336** 9–14

Belan M, Massaglia S, Tordella D, Mirzaei M and de Ponte S 2013 *Astron. Astrophys.* **554** A99

Belan M, Tordella D and De Ponte S 2001 *Proc. 19th ICIASF meeting (Cleveland, OH, USA)* pp 409–16

Bellan P M, Livio M, Kato Y, Lebedev S V, Ray T P, Ferrari A, Hartigan P, Frank A, Foster J M and Nicolaï P 2009 *Phys. Plasmas* **16** 4

Bellan P M, You S and Hsu S C 2005 *Astrophys. Space Sci.* **298** 203

Borkowski K J, Blondin J M and Harrington J P 1997 *Astrophys. J.* **482** L97

de Colle F and Raga A C 2006 *Astron. Astrophys.* **449** 1061

Falize É, Michaut C and Bouquet S 2011 *Astrophys. J.* **730** 96

Gregory C D, Howe J, Loupias B, Myers S, Notley M M, Sakawa Y, Oya A, Kodama R, Koenig M and Woolsey N C 2008 *Astrophys. J.* **676** 420

Godfrey L E H and Shabala S S 2013 *Astrophys. J.* **767** 12

González M, Audit E and Stehlé C 2009 *Astron. Astrophys.* **497** 27

Hartigan P, Foster J M, Wilde B H, Coker B F, Rosen P A, Hansen J F, Blue B E, Williams R J R, Carver R and Frank A 2009 *Astrophys. J.* **705** 1073

Hartigan P, Frank A, Foster J M, Wilde B H, Douglas M, Rosen P A, Coker B F, Blue B E and Hansen J F 2011 *Astrophys. J.* **736** 29

Hodges-Kluck E J and Reynolds C S 2011 *Astrophys. J.* **733** 58

Kössl D and Müller E 1988 *Astron. Astrophys.* **206** 204

Lebedev S V *et al* 2005 *Mon. Not. R. Astron. Soc.* **361** 97

Massaglia S, Bodo G and Ferrari A 1996 *Astron. Astrophys.* **307** 997
Matsakos T, Tsinganos K, Vlahakis N, Massaglia S, Mignone A and Trussoni E 2008 *Astron. Astrophys.* **477** 521
Mundt R, Ray T P and Raga A C 1991 *Astron. Astrophys.* **252** 740
Ray T P, Mundt R, Dyson J E, Falle S A E G and Raga A C 1996 *Astrophys. J.* **468** L103
Reipurth B and Bally J 2001 *Annu. Rev. Astron. Astrophys.* **39** 403
Rus B, Mocek T, Präg A R, Kozlová M, jamelot G, Carillon A, Ros D, Joyeux D and Philippou D 2002 *Phys. Rev.* A **66** 063806
Suzuki-Vidal F *et al* 2010 *Phys. Plasmas* **17** 112708
Tesileanu O, Mignone A and Massaglia S 2008 *Astron. Astrophys.* **488** 429
Tordella D, Belan M, Massaglia S, de Ponte S, Mignone A, Bodenschatz E and Ferrari A 2011 *New J. Phys.* **13** 043011
Tzeferacos P, Ferrari A, Mignone A, Zanni C, Bodo G and Massaglia S 2009 *Mon. Not. R. Astron. Soc.* **400** 820
Zanni C, Bodo G, Rossi P, Massaglia S, Durbala A and Ferrari A 2003 *Astron. Astrophys.* **402** 949
Zanni C, Ferrari A, Rosner R and Massaglia S 2007 *Astron. Astrophys.* **469** 811